HHS Public Access

Author manuscript

Neuroscience. Author manuscript; available in PMC 2017 April 05.

Published in final edited form as:

Neuroscience. 2016 April 05; 319: 206–220. doi:10.1016/j.neuroscience.2016.01.022.

Blast Exposure Causes Dynamic Microglial/Macrophage Responses and Microdomains of Brain Microvessel Dysfunction

Bertrand R. Huber[1], **James S. Meabon**[2,3], **Zachary S. Hoffer**[4], **Jing Zhang**[5], **Jake G. Hoekstra**[5], **Kathleen F. Pagulayan**[2,3], **Pamela J. McMillan**[2,3], **Cynthia L. Mayer**[2,3], **William A. Banks**[6,7], **Brian C. Kraemer**[6,7], **Murray A. Raskind**[2,3], **Dorian B. McGavern**[8], **Elaine R. Peskind**[2,3], and **David G. Cook**[6,7,9]

[1]VA Jamaica Plain, Department of Neurology, Boston University School of Medicine, Jamaica Plain, MA, USA

[2]Northwest Network Mental Illness, Research, Education, and Clinical Center (MIRECC), VA Puget Sound Healthcare Systems, Seattle, WA, USA

[3]Department of Psychiatry and Behavioral Sciences, University of Washington, Seattle, WA, USA

[4]United States Army, Madigan Army Medical Center, Joint Base Lewis-McChord, WA, USA

[5]Department of Pathology, University of Washington School of Medicine, Seattle, WA, USA

[6]Geriatric Research, Education, and Clinical Center (GRECC), Veterans Affairs Puget Sound Health Care System, Seattle, WA, USA

[7]Division of Gerontology and Geriatric Medicine, Department of Medicine, University of Washington, Seattle, WA, USA

[8]National Institute of Neurological Disorders and Stroke, National Institutes of Health, Bethesda, MD, USA

[9]Department of Pharmacology, University of Washington School of Medicine, Seattle, WA

Abstract

Exposure to blast overpressure (BOP) is associated with behavioral, cognitive, and neuroimaging abnormalities. We investigated the dynamic responses of cortical vasculature and its relation to microglia/macrophage activation in mice using intravital two-photon microscopy following mild

Corresponding Author: David G. Cook, PhD, VA Puget Sound Health Care System / Department of Medicine, Univ. of Washington, 1660 S. Columbian Way, Seattle WA 98108, 206-768-5437 (phone), 206-764-2569 (FAX), dgcook@u.washington.edu.

AUTHOR CONTRIBUTIONS

BRH, JSM, ZSH, JGH, PJM, DGC conducted experiments, generated experimental animals/reagents. BRH, JSM, BCK, CLM, DBM, ERP, DGC contributed significantly to study design. BRH, JSM, WAB, BCK, DBM, ERP, DGC performed data analysis and data interpretation. BRH, JSM, KFP, JZ, WAB, BCK, CLM, DBM, ERP, MAR, DGC drafted manuscript and/or revised it critically for important intellectual content.

DISCLOSURE/CONFLICT OF INTEREST

JSM is Chief Operations Officer of Neurogenix Pharmaceuticals. The other authors declare no competing interests

blast exposure. We found that blast caused vascular dysfunction evidenced by microdomains of aberrant vascular permeability. Microglial/macrophage activation was specifically associated with these restricted microdomains, as evidenced by rapid microglial process retraction, increased amoeboid morphology, and escape of blood-borne Q-dot tracers that were internalized in microglial/macrophage cell bodies and phagosome-like compartments. Microdomains of cortical vascular disruption and microglial/macrophage activation were also associated with aberrant tight junction morphology that was more prominent after repetitive (3X) blast exposure. Repetitive, but not single, BOPs also caused TNFα elevation two weeks post-blast. In addition, following a single BOP we found that aberrantly phosphorylated tau rapidly accumulated in perivascular domains, but cleared within four hours, suggesting it was removed from the perivascular area, degraded, and/or dephosphorylated. Taken together these findings argue that mild blast exposure causes an evolving CNS insult that is initiated by discrete disturbances of vascular function, thereby setting the stage for more protracted and more widespread neuroinflammatory responses.

Keywords

blood-brain barrier; two-photon microscopy; neuropathology; microglia; macrophages

INTRODUCTION

Mild traumatic brain injury (mTBI) from blast exposure is the most common form of neurotrauma experienced by military forces in Iraq and Afghanistan (Owens et al., 2008, Bell et al., 2009). Expanded use of improvised explosive devices and multiple deployments have increased the frequency of exposure, while advances in body armor and battlefield medicine have improved survival. Studies of Veterans with repetitive blast-induced mTBI have demonstrated persistent postconcussive symptoms, as well as extensive structural and functional neuroimaging abnormalities (Mac Donald et al., 2011, Jorge et al., 2012, Petrie et al., 2014). Moreover, the neuropathology of chronic traumatic encephalopathy (CTE) has been reported in Iraq Veterans with a history of blast injury (Omalu et al., 2011, Goldstein et al., 2012, McKee et al., 2013).

Growing evidence indicates that blast exposure is capable of disrupting cortical vessels forming the blood brain barrier (BBB), provoking microglial/macrophage activation. An initial mechanism of blast-induced vascular disruption is thought to involve physical damage to vessels from mechanical forces leading to oxidative damage and reduced expression of tight junction proteins (Abdul-Muneer et al., 2013). However, the real-time dynamic responses of CNS microvasculature and microglia/macrophages to blast-induced mTBI have not been reported. Non-blast CNS injury approaches have been shown to activate microglia/macrophages, which mobilize to the site of injury (Nimmerjahn et al., 2004, Roth et al., 2014) recruiting peripheral monocytes and neutrophils to assist in the elimination of damaged tissue (Shechter et al., 2009, London et al., 2011). Depending on the method of injury, BBB disruption can result in either rapid or delayed glial responses (Nimmerjahn et al., 2005, Seiffert et al., 2004). *In vivo* studies of skull depression-induced TBI demonstrate microglia with extended, enlarged, and flattened processes that form confluent sheets over the area of injury (Roth et al., 2014). Focal disruption of vessels with targeted laser pulses

also causes microglial migration to the site of injury, where microglia shield injured vessels from the surrounding parenchyma (Nimmerjahn et al., 2005). These *in vivo* models suggest that microglia form barriers at sites of injury, particularly in regions adjacent to the glial limitans.

Accumulating evidence suggests that blast exposure provokes pathophysiological responses that can be distinct from non-blast TBI (Elder et al., 2014). Thus, to better understand the dynamic pathophysiological underpinnings of blast-related mTBI we have used our established murine model of blast-induced mTBI (Huber et al., 2013) to examine the early-occurring dynamic relationships between vascular disruption and microglia/macrophage responses to mild BOP using real-time *in vivo* two-photon microscopy via a thinned skull imaging methodology. Thinned skull preparations result in little or no inflammation of the underlying cortex, thereby allowing study of the native response of microglia to blast induced vascular permeability (Davalos et al., 2005, Xu et al., 2007, Yang et al., 2010). Using this approach, we have found that mild blast exposures that are comparable to those commonly experienced by military service members provoke discrete microdomains of vascular dysfunction and correspondingly discrete microglial/macrophage responses that are associated with aberrant tight junction morphology.

EXPERIMENTAL PROCEDURES

Shock tube

The shock tube was designed to generate shock waves that replicate combat-relevant forces produced by open-field high-explosive detonations (Baker Engineering and Risk Consultants, San Antonio, TX). The characteristics and operational properties of the shock tube are described in detail elsewhere (Huber et al., 2013). Briefly, the shock tube consists of a variable volume driver that controls primary positive peak duration. A dual diaphragm spool distributes the pressure difference between the driver and driven section of the tube across two membranes. The shock tube is activated by rapidly releasing the pressure between the two diaphragms causing rupture of both diaphragms via a remotely controlled high-speed electronic valve. Static pressure measurements were recorded via three side-mounted pressure sensors (PCB Piezoelectronics, Depew, NY) positioned 89 cm upstream, 89 cm downstream, and adjacent to the animal harness. Pressure sensor data were collected at 20 kHz with a National Instruments analog-to-digital data acquisition unit (Austin, TX) and processed using a custom LabVIEW interface (National Instruments, Austin, TX). The end of the shock tube is fitted with an attenuator that reduces ambient transient blast noise to less than 100 decibels and suppresses reflected shock waves.

Animals and blast parameters

Where indicated in the Results Section, 3–4 month old male CX3CR1-GFP$^{+/-}$ (n=14) or wild type C57BL/6 (n= 80) mice (Jackson Laboratories) were used for this study. All mice had *ad libitum* access to food and water, were maintained under specific antigen-free (SPF) conditions with a 12/12 hour day/night cycle, and housed 2–4 per cage. All animals were housed and handled in accordance with protocols approved by the Veterans Affairs Puget Sound Health Care System's Institutional Animal Care and Use Committee (IACUC) and all

experiments were conducted in accordance with the National Institutes of Health Guide for the Care and Use of Laboratory Animals. Experiment group sample sizes were based on prior pathologic findings (Huber et al., 2013). All mice were allowed to acclimatize to the animal facility for at least one week prior to blast exposure. In preparation for blast exposure, animals were anesthetized with 2% isoflurane delivered with a non-rebreathing anesthesia machine at a flow rate of 1 L/min oxygen after initial induction with 5% isoflurane. A flexible custom facemask designed to fit over the nose and mouth was attached to the mouse harness and provided anesthesia during blast exposure or sham treatment. Mice were warmed on a heating pad (Gaymar, Orchard Park, NY) while anesthetized, except for the 2–5 minutes spent in the shock tube (the time required to position the animal, pressurize the driver, deliver blast overpressure [BOP], and remove the animal). To minimize blast-induced head and body motion, the mice were securely mounted using plastic cable ties that attached each limb to a steel frame restraint harness supporting an open ¼-inch rigid mesh. Aiming to reproduce a common occurring in-theater scenario where the military service member is facing the incoming shock wave with the torso turned toward the shock wave front, the animals' ventral body surface was oriented perpendicular with respect to the oncoming blast wave in accordance with well-established methods (Koliatsos et al., 2011). Each BOP-exposed animal was followed by a yoked non-blasted sham control animal that was mounted in the restraint harness and held under anesthesia for the same amount of time as its paired BOP-exposed mouse, hence treatment selection was not randomized. The BOP used in these experiments had a peak static pressure of 15.3 psi (s.e.m. +/− 0.25), a positive phase duration of 5.78×10^{-3} sec (s.e.m. +/− 1.31×10^{-4}), with a resulting impulse of 2.55×10^{-2} psi*sec (s.e.m. +/− 5.34×10^{-4}), and a shock wave velocity of 1.4 Mach. Mice that were used for Western blotting or immunohistochemistry were immediately removed from the shock tube following blast exposure or sham treatment and placed in a partially heated observation enclosure (37°C). Animals were observed for one-hour to identify evidence of distress. Mice exposed to multiple BOP were housed in the animal facility after the one hour observation period and allowed to recover 24 hours between exposures. Non-blasted sham control mice were mounted onto the shock tube restraint harness under anesthesia the same number of times and for the same duration as the BOP-exposed mice. BOP-exposed and sham treated control mice used for *in vivo* imaging were not yoked, and instead followed the protocol described below. At the conclusion of experiments, animals were euthanized.

Thinned skull surgery

After induction of anesthesia and immediately prior to blast exposure or sham treatment, 30 μl of non-targeted Quantum Dots-655 nm ($QDots_{655}$) (Qtracker, Life Technology, Grand Island, NY) were injected into the retro-orbital sinus of the anesthetized mouse. After blast exposure or sham treatment a thinned skull surgical preparation was performed and the mouse was placed in a custom frame for imaging. This process typically took less than 45 minutes from blast/sham treatment to the beginning of image acquisition. To carry out thinned skull surgery and two-photon microscopy, mice were anesthetized with isoflurane (5% for induction; 1.5–2% for surgery with ~0.5 L/min O_2). The head was shaved and the mouse placed on a heating blanket. The eyes were protected from dehydration with eye-ointment. The scalp was washed with three alternating swabs of 70% ethanol and betadine. Sterile surgical tools were used throughout the protocol. A midline scalp incision was made

extending from the neck region between the ears to the frontal area between the eyes. The periosteum of the skull was removed. A mark was made 2 mm lateral to the sagittal suture and 2 mm caudal to the coronal suture. A small amount of cyanoacrylate glue was placed around the aperture in the mouse holder and the holder was pressed against the skull over the mark for at least 30 seconds. The holder was then inserted into the frame. A 0.5–1 mm^2 area of skull was thinned under the dissecting microscope using a high-speed micro-drill. The drilling was done using a few drops artificial cerebrospinal fluid (119mM NaCl, 26.2mM $NaHCO_3$, 2.5mM KCl, 1mM NaH_2PO_4,1.3mM $MgCl_2$, 1.2mM $CaCl_2$, 0.4% glucose, pH 7.4) intermittently to avoid overheating. Drilling continued until the majority of the spongy bone was removed to a depth of approximately 50 μm. The preparation was repeatedly examined at this point under a microscope as small amounts of bone were removed. At 20–30μm, the underlying fluorescent structures were visible. The bone was polished with an ophthalmic scalpel by gently scraping, without downward pressure, to the surface of the bone. The mouse was maintained on 1.5–2% isoflurane with 0.5 L/min O_2 and then placed in the heated enclosure attached to the two-photon microscope. A small pool of artificial CSF was placed in reservoir above the area of skull thinning and imaging was performed. All animals survived blast and/or sham treatment. For subsequent inclusion in imaging experiments (3/14) animals were excluded from study because of accidental breaching of the skull or evidence of drill-related thermal damage (blood clot formation in the most superficial vessels).

Two-photon imaging and analysis

The anesthetized mouse was placed in a harness that was attached to the TCS SP5 II two photon microscope (Leica, Buffalo Grove, IL). Epifluorescence illumination was used to locate the imaging site. A low resolution scouting Z-stack was obtained to determine the dimension of the Z-stack and to identify a region of interest. Imaging was performed using 1024 × 1024 resolution Z-planes taken at 2 μm intervals, with the least available zoom (1.7×) enabling the largest field of view. To obtain image series over more extended periods of up to 6 hours without inducing tissue injury from over-scanning, one complete Z-stack was imaged every 10 minutes. All *in vivo* imaging was carried out in a temperature controlled (37°C) chamber that enclosed the animal, microscope stage and objectives. All quantitative analyses and data processing were performed using Imaris 7.2 software (Bitplane, Zurich, Switzerland). Microglial filament representations were generated using the Imaris ‘filament’ tool. Microglia start points were automatically generated and subsequently manually curated. The remaining filament building was performed automatically by Imaris. A second manual curation step was performed to ensure accurate filament representations. Microglial convex hull surfaces were generated with Imaris using the ‘convex hull’ add-on written with Matlab (MathWorks, Natick, MA). Colocalization of microglia with $Qdots_{655}$ was performed using the Imaris ‘colocalization’ tool. All analyses were performed non-blinded using identical imaging conditions and image adjustments (limited to linear contrast and brightness adjustments) on datasets from blast and sham-treated animals.

Immunofluorescence and immunohistochemistry

Studies of microvascular permeability to dextran were performed by injecting 100 μl of 400 mg/ml 10 kDa dextran labeled with tetramethylrhodamine (Life Technology, Grand Island, NY) into the retro-orbital sinus after isoflurane induction immediately before BOP exposure or sham treatment. At specified study endpoints/time points mice were humanely euthanized with pentobarbital (300 mg/kg) and transcardially perfused with ice cold 4% paraformaldehyde in phosphate buffered saline (PBS) after cardiac arrest. Confocal microscopy was performed using the same TCS SP5 II two photon microscope as above with Leica objectives (10X, 20X, and 20X-imersion, 0.3, 0.7, and 1.0 numerical aperture, respectively). Brains were post-fixed overnight in 4% paraformaldehyde in PBS at 4°C and then equilibrated with cryoprotectant (30% sucrose in PBS) at 4°C. Sagittal sections embedded in OCT (Tissue-Tek, Torrance, CA) were cut at 50 μm thickness from bisected brains with a CM1850UV cryostat (Leica, Buffalo Grove, IL). The sections were stored at −20°C in cryoprotectant (30% sucrose, 30% ethylene glycol, 1% polyvinylpyrolidone, 0.05M phosphate buffer pH 7.4) for up to 6 months until analyzed and analyzed at room temperature. Antigen retrieval was performed by washing the sections in PBS (3 × 5 min), transferring them to 50 mM sodium citrate (pH 9.0) and then heating at 80°C for 30 minutes. (Jiao et al., 1999) Sections cooled to room temperature were washed (3 × 5 min) in PBS. Sections to be immunostained with antibodies generated in mice were stained using the mouse on mouse kit (Vector Laboratories, Burlingame, CA) in accordance with the manufacturer's recommendations using a one hour incubation with primary antibody. Immunostaining conditions without mouse primary antibodies were stained according to our previously published method.(Huber et al., 2013) Floating tissue sections were cover slipped with a drop of Prolong® Gold Antifade Reagent with or without DAPI (Life Technologies, Grand Island, NY). The following antibodies were used: mouse anti-claudin-5 labeled with Alexa 488 (Life Technologies, Grand Island, NY), rabbit anti-Iba-1 (Wako, Richmond, VA), chicken anti-GFAP (Millipore, Billerica, MA), chicken anti-laminin (Abcam, Cambridge, MA), mouse anti-phospho-tau 396 (Life Technologies, Grand Island, NY), rabbit anti-phospho-tau 396 (AnaSpec, Freemont, CA). Goat secondary antibodies labeled with Alexa 488, Alexa 647 and Cy3 were obtained from Jackson Immunoresearch (West Grove, PA). The sections were imaged with a TCS SP5 II confocal microscope (Leica, Buffalo Grove, IL). All quantitative analyses and data processing were performed using Imaris 7.2 software (Bitplane, Zurich, Switzerland). Microglial filament representations were generated using the Imaris 'filament' tool using the same protocol described for two-photon microscopy. Only microglia fully represented in the 50 μm tissue sections were used for morphological evaluation. Microglial convex hull surfaces were generated with Imaris using the 'convex hull' add-on written with Matlab (MathWorks, Natick, MA). Iba-1 positive microglial process density at one and four hours post blast exposure was quantified by semi-automated Sholl analysis performed with Imaris software. For immunohistochemistry 10 μm sections were deparaffinized in xylene and rehydrated through graded alcohols to water. Sections were treated for endogenous peroxidases with 3% hydrogen peroxide, blocked in 5% milk, incubated with primary antibody (Anti-Tau pSer396, AnaSpec) overnight at 4°C, followed by biotinylated secondary antibody for 45 minutes at room temperature. Finally, sections were incubated in an avidin-biotin complex (Vectastain Elite ABC kit, Burlingame, CA) and

the reaction product was visualized with 0.05% diaminobenzidine (DAB)/0.01% hydrogen peroxide in PBS.

Western blots

Brains were immediately dissected in ice cold PBS and then cortices were sub-dissected. Tissue lysates were then prepared as previously described.(Huber et al., 2013) Tissues were manually homogenized twice using an Eppendorf tube-fitting pestle (Eppendorf, Hauppauge, NY) before centrifuge clarification. Criterion 4–20% TGX gels (Bio-Rad, Hercules, CA) were loaded with 20 μg/lane and probed once after overnight incubation (4°C) with the following antibodies: mouse anti-phospho-tau 396 (Life Technologies, Grand Island, NY), rabbit anti-phospho-tau 396 (from AnaSpec, Freemont, CA), AT270 (from Thermo Scientific, Waltham, MA), tau-5 (Life Technologies, Grand Island, NY), TNFα (Abbiotec, San Diego, CA). Probes for total tau levels and/or pyruvate kinase (Rockland, Gilbertsville, PA) were conducted similarly after stripping. Target bands were analyzed by densitometry with ImageQuant TL (GE, Piscataway, NJ). Tau epitope-specific levels were standardized by total tau levels, and blast condition-values were normalized to identically calculated controls.

Statistics

Where indicated standard t-test statistics were used with *p* values indicating two-tailed critical values corresponding to $p \leq 0.05$. Error bars indicate standard error of the mean (s.e.m.).

RESULTS

Mild blast exposure induces transient microdomains of BBB disruption

A pneumatic shock tube (see Methods and Huber et al., 2013) was used to expose mice to mild BOP (peak amplitude = 15.3 psi, s.e.m.. +/− 0.25; positive phase duration = 5.78×10^{-3} sec +/− 1.31×10^{-4}; impulse = 2.55×10^{-2} psi*sec +/− 5.34×10^{-4} N= 22) corresponding to an open field TNT detonation of approximately 16 kg at a distance of 7.6 m. As in our previous experiments (Huber et al., 2013), all of the blast-exposed mice survived, including animals that received as many as three BOP (with a 24 hour inter-blast interval) inspected as long as 14 days post-exposure and gross histological examination revealed no instances of skull fractures, no overt central nervous system (CNS) contusions or hemorrhages, and no apparent gross injury or disruption of the subarachnoid vasculature compared to sham control animals.

To examine the effect of mild blast exposure on brain microvascular permeability we used real-time two-photon intravital microscopy via a thinned skull preparation overlying the medial cortex (approximately 2 mm lateral and 2 mm posterior to bregma). To image microvascular integrity after blast exposure, $Qdots_{655}$ that were 15–20 nm in diameter (hydrodynamic size comparable to a 500kDa globular macromolecule) were retro-orbitally loaded immediately prior to blast or sham control treatment. Figure 1 shows that after a single mild blast we observed increased vascular permeability of $Qdots_{655}$ imaged as they crossed the endothelium into the surrounding parenchyma from 45 minutes to 105 minutes

post-blast exposure (skull thinning was carried out immediately after the blast exposure or sham treatment). Increased aberrant microvascular permeability was observed in 100% (6/6) of the blast exposed mice, while $Qdots_{655}$ remained confined to the intravascular luminal space in 100% (4/4) of the sham-treated control mice. $Qdots_{655}$ escaping the vascular lumen accumulated predominantly in the subpial space adjacent to the glial limitans superficialis (Figure 1). Mild blast exposure induced a distinct pattern of regionally and temporally restricted vascular disruption. Microdomains of vascular disruption averaged 256 μm ± 23 μm (s.e.m.) in diameter (9 regions of vascular disruption identified in 6 blast exposed animals) and typically lasted for 1–2 hours. Figure 1 (lower panel) shows a specific vascular microdomain of disruption in the top right (white arrow heads) of the imaging field that abated over the imaging session, while a second microdomain in the lower middle region of the imaging field (green arrow heads) emerged later within 65 minutes post-blast.

These results indicate that mild blast exposure creates transient and highly localized microdomains of vascular permeability leading to perivascular accumulation of $Qdots_{655}$ in the absence of vascular hemorrhage or thrombosis. In addition, these findings also indicate that vascular disruption continues to develop hours after the initial BOP, suggesting that under mild blast exposure conditions vascular dysfunction was unlikely to be due simply to immediate mechanical microvessel tearing or shearing.

Blast exposure leads to microglial activation and uptake of leaked Qdots

Multiple reports indicate that blast exposure induces microglial activation (Readnower et al., 2010, Goldstein et al., 2012, Perez-Polo et al., 2013). However, the relationship between blast-induced vascular disruption and microglial/macrophage activation is not well understood. To test whether blast-induced vascular permeability is spatially and temporally associated with microglial/macrophage activation, we used CX3CR1-$GFP^{+/-}$ mice that express green fluorescent protein (GFP) in microglia and other monocyte/macrophage lineage cells (Jung et al., 2000, Roth et al., 2014). Morphological changes indicative of microglial/macrophage activation include decreased process length, retraction or shortening of processes, and increased cell body size (Nimmerjahn et al., 2005). Figure 2 shows that a single mild blast caused microglial/macrophage activation characterized by significantly decreased summed filament length in blast-exposed mice compared to shams (328.59 ± 17.48 μm and 441.40 ± 27.32 μm, N= 6 and 4, blast-exposed and shams, respectively; $t[8] = -3.67$, $p<0.006$). In addition, process retraction was examined by convex hull volume analysis, which estimates the volume created by forming a convex envelope containing all of the cellular filaments. By this method of analysis activated microglia with retracted filaments are expected to result in smaller convex hull volumes (Figure 2A). In keeping with this we found that blast exposure significantly decreased mean convex hull volume in BOP-exposed mice compared to sham controls (Figure 2B) (12675.1 ± 2674.18 μm^3 and 23812.80 ± 2584.50 μm^3, N= 6 and 4, blast-exposed and shams, respectively; $t[8] = -2.84$, $p<0.022$). This further confirms that single mild blast caused dynamic microglial process retraction and adoption of a more amoeboid morphology within 45 minutes.

These blast-induced morphological changes in microglial/macrophages appeared to be associated specifically with microdomains of vascular disruption in 100% (6/6) blast-

exposed mice 45 minutes after BOP exposure (Figure 2C). Figure 2C also shows that in the same blast-exposed mouse, GFP-expressing microglia/macrophages located approximately 100 μm or more from the vascular-disruption microdomain in Figure 2C (lower panel) appeared markedly more ramified and less amoeboid, indicating a lesser degree of activation compared to nearby microglia/macrophages localized within the domain of vascular disruption shown in the middle panel of Figure 2C.

Microglia/macrophages avidly internalized $Qdots_{655}$ crossing the endothelium into enlarged perivascular processes and cell bodies. Figures 3A and 3B show that a single mild blast led to a significant increase in apparent Qdot internalization within microglia/macrophages (white arrows) in BOP-exposed animals (0.18% ± 0.044) co-localized fluorescence compared to sham treated animals (0.018% ± 0.005; N= 6 and 4, blast and shams, respectively, $t[8] = 2.99$, $p \leq 0.02$). The phagocytosed $QDots_{655}$ frequently accumulated in enlarged perivascular processes extending from a microglia cell body (Figure 3C). These enlarged perivascular processes had the morphology of phagosomes,(Nimmerjahn et al., 2005) and usually lasted approximately two hours, and then dispersed into filament-like projections. To confirm that apparent QDot co-localization within these small GFP-expressing cells was not due to non-specific auto-fluorescence, as a control we imaged a CX3CR1-$GFP^{+/-}$ mouse without $QDots_{655}$ and detected negligible autofluorescence in the 645–670nm spectral window used to detect the $QDots_{655}$ (Figure 3D).

Taken together these results indicate that mild blast exposure causes discrete microdomains of vascular disruption that are associated with corresponding subdomains of microglial/macrophage activation evidenced by decreased microglial process length, reduced convex hull envelope volume, and microglial/macrophage phagocytosis of $Qdots_{655}$ crossing the endothelium. As little as 100 μm away from the margin of vascular disruption microdomains microglial/macrophage activation was less pronounced, suggesting that early-occurring disturbances in vascular integrity play an important role in defining dynamic region-specific microglial/macrophage activation responses to mild blast exposure within the timeframe examined.

Mild blast exposure leads to tight junction injury

To determine whether blast-induced vascular-disruption was associated with brain microvessel endothelial tight junction disturbances, we retro-orbitally loaded the blood supply of mice with Texas Red-conjugated 10 kDa dextran immediately prior to blast or sham treatment. Confocal microscopy was carried out on cortex from sham and blast-exposed mice after PBS clearance of peripheral circulating dextran in order to label microdomains where dextran had escaped across the BBB into the CNS parenchyma. All images in Figure 4 show maximum-field projections of 40 serially acquired images scanned at 1μm intervals in the Z-plane (40 μm total tissue thickness). Figure 4A shows that one hour following a single mild BOP, the immunostaining pattern of claudin-5, a transmembrane tight junction protein required for vascular functional integrity (Nitta et al., 2003) (pseudo colored as white) was: (i) disturbed compared to shams; (ii) associated with leakage of 10 kDa dextran (red); and (iii) colocalized with Iba-1 positive (green) microglial/macrophages (arrowheads). This finding of aberrant tight junction morphology co-localized with

microdomains of vascular leakage and microglial/macrophage dextran uptake was observed only in blast-exposed mice and not in controls (100%, n=5/5 and 0% N=0/5 of shams). We also examined tight junction morphology 24 hours after single (1X) or triple (3X) BOP exposures (24 hour inter-BOP interval). As above (Figure 4A), in sham-treated animals (Figure 4B) tight junctions in cortical penetrating vessels were clearly delineated by distinct claudin-5 immuno-positive endothelial cell-to-cell junctions. In contrast to the results obtained at one hour, the morphologic pattern of claudin-5 immunostaining in 1X blast-exposed mice had largely returned to normal and, with the exception of isolated instances (Figure 4B left most panels), was comparable to shams. In contrast to this, 24 hours after 3X BOP exposure claudin-5 tight junction staining appeared discontinuous and irregular in 60% (n=3/5). While these data indicate that a single mild blast causes transiently abnormal tight junction morphology, Figure 4C shows that one hour following a single blast, peripherally injected 10kDa Dextran (which is much smaller than Q-dots) can nonetheless escape into the CNS parenchyma.

Taken together these findings indicate that even a single mild blast exposure is capable of transiently disturbing tight junction morphology that is coupled with vascular dysfunction. In addition, repetitive, but not single blast exposure is associated with longer lasting aberrant claudin-5 expression.

Blast exposure causes microglial activation at deeper levels of the cortex

The *in vivo* findings indicate that mild blast exposure causes rapid microglial activation (Figures 1–3) in the superficial layers of cortex that are amenable to analysis by two-photon intravital imaging. Both to confirm these findings by an alternate experimental approach and to also address whether microglia located deeper within the cortex (~150 μm to 500 μm below the cortical surface) are similarly activated by mild BOP, we quantified normalized microglial filament length and convex hull volume in perfusion-fixed, Iba-1 immunostained cortical tissue sections from wild-type C57BL6 mice. Microglia in the blast-exposed mice appeared less ramified (Figure 5A) and the calculated convex hull volume was reduced in the cortical gray matter compared to shams (Figure 5B). At both 1 and 4 hours after a single mild BOP, microglial filament length and convex hull volume (Figure 5C, D) were significantly reduced compared to shams (normalized filament length at 1 hour: 1.0 ± 0.06 μm and 0.78 ± 0.07 μm, N=5 and 5, sham and BOP, respectively; t[8]=−2.45, $p<0.04$; normalized filament length 4 hours: 1.0 ± 0.06 μm and 0.69 ± 0.06 μm, N= 4 and 4, blast-exposed and shams, respectively; t[6]= −2.99, $p<0.03$; convex hull volume at 1 hour: 1.0 ± 0.08 μm^3 and 0.73 ± 0.07 μm^3, N= 5 and 5, sham and BOP respectively; t[8]=−2.51, $p<0.04$; convex hull volume at 4 hours: 1.0 ± 0.02 μm^3 and 0.75 ± 0.06 μm^3, N=4 and 4, shams and BOP, respectively, t[6]=−3.30, $p<0.02$). A Sholl analysis of Iba-1 positive microglial processes at one and four hours post blast or sham treatment revealed a statistically significant decrease in average process crossings in blast-exposed mice. A three-factor ANOVA (treatment: blast vs sham, post-treatment interval:1 versus 4 hours, and Sholl radii 5–35μm as a repeated measures factor) was performed with an average of 119.6 cells analyzed per animal (n=5 per group). Blast exposure caused a statistically significant overall decrease in process density compared to shams ($F[1,16]= 6.448$ $p<= 0.022$), with overall process density greatest at the 1 hour time point ($F[1,16]=32.551$, $p<= 0.001$)(Figure 5E, F).

Taken together these data argue that microglia/macrophage rapidly adopt an activated-appearing morphology in response to a mild blast exposure.

Phosphorylated tau accumulates acutely around vessels after blast exposure

To address the possibility that mild blast exposure may alter perivascular phospho-tau expression in blast exposed mice we performed confocal microscopy using a well-characterized mouse phospho-tau monoclonal antibody (pS396) (Hoffmann et al., 1997, Bennett et al., 2013, Kim et al., 2014). We found aberrant phospho-tau accumulation in perivascular regions of non-penetrating small (~8–15 μm diameter) cortical microvessels in 100% (n=5/5) of BOP-exposed mice and none (n=0/5) of the sham treated mice at 1 hour post-exposure (Figure 6A). We further confirmed the presence of blast-induced perivascular phospho-tau expression using a rabbit polyclonal antibody also raised against the phospho-tau S396 epitope (Figure 6B). To validate the specificity of this rabbit anti-tau pS396 antibody we confirmed that it recognized tau deposits in cortex of transgenic tau-P301S mutant (PS19) mice (Yoshiyama et al., 2007) and was immuno-negative in non-transgenic mice, as well as tau knock-out (KO) mouse brain tissue (Figure 6C). Perivascular phospho-tau expression was not found at later time points (4 hours), suggesting that phospho-tau is dephosphorylated, degraded, or cleared from this anatomic compartment within four hours under our mild BOP exposure conditions. While pS396 was the only phospho-tau species we found to be elevated in perivascular spaces by confocal microscopy, Western blot analysis confirmed that this species of phospho-tau, as well as others, were aberrantly elevated in cortex following a single mild blast exposure (Figure 6D). Taken together this indicates that even though BOP induces marked increases in aberrant phospho-tau, under these mild exposure conditions, perivascular blast-induced phospho-tau rapidly returned to control levels.

Repetitive BOP causes increased TNFα levels and microglia density

To determine if repetitive BOP exposure leads to more protracted alterations in microglial function we quantified TNFα levels in cortical protein lysates at two weeks after 1X and 3X blast exposures. TNFα is associated with microglial activation and neuronal injury (Zujovic et al., 2000). Figure 7 shows that at 14 days post blast or sham exposure only the repetitively (3X) exposed animals demonstrated a statistically significant increase in TNFα expression (1.92 ± 0.24 and 1.0 ± 0.28, N=5 and 5 3X BOP and shams, respectively; $t[8] = 2.85$, $p<0.05$). Consistent with this finding, cortical microglial counts were significantly increased in 3X blast-exposed mice compared to shams (102.6 ± 2.96 and 92.6 ± 1.11, N=5 and 5, 3X BOP and shams, respectively; $t[8] = 2.40$, $p \leq 0.05$), but not in 1X BOP exposed mice (96 ± 4.72 and 99.2 ± 4.14, N=5 and 5, 1X BOP and shams, respectively; $t[8] = -0.51$, n.s). These data suggest that repetitive BOP exposure promotes increasingly persistent neuroinflammatory changes in the CNS.

DISCUSSION

These results provide *in vivo* evidence that mild blast causes regional and transitory disruptions in penetrating arteries and cortical vessels, generating microdomains of increased permeability that are associated with microglial/macrophage activation. This

pattern of injury was found throughout the cortex and is unlike the focal pattern of injury observed in other models of TBI such as fluid percussion injury, (Hayes et al., 1987) controlled cortical impact, (Lighthall, 1988) and skull depression (Roth et al., 2014). In blast-exposed mice, blood-borne $Qdots_{655}$ and 10 kDa dextran are released in focal perivascular microdomains in association with activated local microglia/macrophages that we found throughout the cortex, but were most prevalent near the cortical surface. The perivascular pattern of activation is similar to the pattern generated by laser pulse-induced vascular permeability (Nimmerjahn et al., 2005).This suggests that the source of microglial activation may be transitory disruption of the endothelium and/or secondary reactions associated with inflammatory mediators. The finding of focally disrupted claudin-5 morphology, both at the surface of the cortex, as well at deeper cortical levels hours after BOP exposure suggests that tight junction dysfunction plays a role in BOP-induced vascular permeability. Moreover, these data suggest that aberrant tight junction morphology is more prominent and persistent following repetitive blast exposure.

We observed a wide range of activated microglia/macrophage morphologies associated with disturbed vascular permeability, ranging from amoeboid cells with retracted processes to hyper-ramified cells with enlarged and extended processes. This range of morphology was similar to other *in vivo* studies of microglial/macrophage activation (Morrison and Filosa, 2013). Microglial amoeboid morphology is associated with ongoing neuroinflammatory processes and is linked to the release of pro-inflammatory molecules such as TNFα (McPherson et al., 2014). In addition, there are numerous examples of enlarged phagocytic perivascular processes (Nimmerjahn et al., 2005). The enlarged perivascular processes actively take up leaked $Qdots_{655}$ from the surrounding parenchyma and concentrate them in the center of the process, as well as in the cell bodies of the microglia/macrophages.

Activation and infiltration of microglia and macrophages are common features of TBI involving focal injury (Wang et al., 2013). However, each of these models of TBI generates a single focus of cortical injury that is less similar to this model of blast injury, which generates multifocal cortical vasculopathy. The focal injury pattern seen in other models of TBI is associated with a nidus of neuroinflammation composed of activated microglia and macrophages. Conversely, in blast-induced TBI many cortical vessels are damaged, leading to multiple microdomains of vascular disruption with perivascular cuffs of CX3CR1-GFP positive cells. The perivascular cuffs are composed of cells with amoeboid morphology and partially ramified microglia with thickened processes extending into the cuff. A limitation of using CX3CR1-GFP mice is that microglia that have adopted an amoeboid morphology cannot be reliably distinguished from macrophages, therefore it is unclear if the perivascular cells with amoeboid morphology are macrophages or activated microglia that have become fully de-ramified.

One challenging aspect in identifying the cellular constituents associated with specific regions of injury is the difficulty of clearly distinguishing the myeloid lineage cells that are labeled by the CX3CR1-$GFP^{+/-}$ mice. In these mice, microglia, monocytes, and perivascular macrophages all express GFP (Jung et al., 2000). Moreover, all of these cell types are recruited to sites of injury. Distinguishing among these cell types based on morphology is also not reliable because activation can cause microglia to adopt a more de-ramified

morphology similar to macrophages and monocytes. Nonetheless, the CX3CR1-GFP$^{+/-}$ mice permitted a clear demonstration that mild BOP produces discrete sub-regions of microglial/macrophage activation and/or infiltration that is both temporally and spatially linked to cortical vascular disruption.

These results indicate that previous blast exposure (i.e., repetitive blasts) may potentiate longer-lasting microglial activation responses reflected by increased TNFα levels and increased numbers of microglia two weeks after blast exposure. This raises the possibility that repetitive BOP sets the stage for longer term neuroinflammatory reactions as the number of blast-related insults increases.

In this study, intravital two-photon microscopy of blast-exposed mice demonstrated that $Qdots_{655}$ accumulate in the Virchow-Robin space, which is a CSF-filled space between the vessels and the glia limitans. These results were observed in both CX3CR1-GFP$^{+/-}$ and wild-type C57BL6 mice via intravital imaging and were also confirmed using standard confocal microscopic approaches on fixed tissue sections. This confirms that the vascular disruption findings observed in the CX3CR1-GFP$^{+/-}$ mice were not likely related to CX3CR1 heterozygosity.

Perivascular tau has been observed in individuals with CTE (Omalu et al., 2011, Goldstein et al., 2012). In these cases, hyper-phosphorylated tau accumulates in the perivascular astrocytes and neuropil of the glial limitans. BOP-exposed mice demonstrate accumulation of phosphorylated tau, specifically tau phosphorylated at S396 surrounding vessels throughout the cortex. Perivascular tau was observed for a short time after BOP-exposure and was not observed by 4 hours post-blast. While the specificity of this perivascular phospho-tau immunoreactivity was rigorously confirmed, it nonetheless did not appear to be associated with a particular cell type. Instead, it appeared to be associated with the glia limitans aspect of the Virchow-Robin space.

When considered together, these findings suggest that mild blast exposure causes a release of aberrant phospho-tau that may be rapidly transported to the Virchow-Robin space and then eliminated via the CSF (Iliff et al., 2012). This idea is consistent with our previous findings of increased phospho-tau levels in mice after blast exposure (Huber et al., 2013) and by the significantly elevated tau levels reported in individuals that have experienced severe TBI (Magnoni et al., 2012). That the blast-induced perivascular tau accumulation we reported in blasted mice is quite transitory suggests that under these experimental conditions, the required use of anesthesia may have been a factor that potentiated rapid tau clearance (Xie et al., 2013).

Collectively these findings are consistent with the possibility that vascular-related clearance may be an important means of eliminating the substantial levels of aberrant phospho-tau (Figure 6) that rapidly accumulate following even a single mild blast exposure. Numerous other TBI-related substances have been shown to clear the brain by similar means, (Plog et al., 2015) thus further emphasizing the potential importance of early-occurring blast-induced vascular disturbances in the pathological long-term consequences of blast-related mTBI

regardless whether or not phospho-tau specifically accumulates chronically in blast-exposed humans or mice.

In summary, these findings demonstrate that mild blast exposure produces highly localized, aberrant cortical vascular permeability that is closely associated with sites of microglial/macrophage activation. To our knowledge these are the first reported intravital imaging studies carried out in blast-exposed mice and, albeit short-lived under our experimental conditions (~ 1 hour), the first demonstration of blast-induced aberrant perivascular phospho-tau accumulation. We also find that repetitive mild blast exposure leads to longer lasting neuroinflammatory changes, including elevated TNFα levels and increased density of microglia two weeks following blast exposure.

Acknowledgments

This work was supported by the Department of Veterans Affairs Office of Research and Development Medical Research Service (DGC, ERP, BCK, WAB), University of Washington Friends of Alzheimer's Research (DGC, ERP), University of Washington Royalty Research Fund (DGC); R01AG046619 (WAB); Northwest Network Mental Illness Research, Education and Clinical Center (ERP, BRH, JSM, KFP, PJM, CLM), Office of Academic Affiliations, Advanced Fellowship Program in Mental Illness Research and Treatment, Department of Veterans Affairs (BRH); NIH T32 AG000258 (JSM), VA CSR&D Career Development Award Program #IK2 CX00516 (KFP). We thank Dr. Gerard Schellenberg (Univ. Pennsylvania) for providing Tau knock out samples.

REFERENCES

Abdul-Muneer PM, Schuetz H, Wang F, Skotak M, Jones J, Gorantla S, Zimmerman MC, Chandra N, Haorah J. Induction of oxidative and nitrosative damage leads to cerebrovascular inflammation in an animal model of mild traumatic brain injury induced by primary blast. Free radical biology & medicine. 2013; 60:282–291. [PubMed: 23466554]

Bell RS, Vo AH, Neal CJ, Tigno J, Roberts R, Mossop C, Dunne JR, Armonda RA. Military traumatic brain and spinal column injury: a 5-year study of the impact blast and other military grade weaponry on the central nervous system. The Journal of trauma. 2009; 66:S104–S111. [PubMed: 19359953]

Bennett RE, Esparza TJ, Lewis HA, Kim E, Mac Donald CL, Sullivan PM, Brody DL. Human apolipoprotein E4 worsens acute axonal pathology but not amyloid-beta immunoreactivity after traumatic brain injury in 3xTG-AD mice. Journal of neuropathology and experimental neurology. 2013; 72:396–403. [PubMed: 23584199]

Davalos D, Grutzendler J, Yang G, Kim JV, Zuo Y, Jung S, Littman DR, Dustin ML, Gan WB. ATP mediates rapid microglial response to local brain injury in vivo. Nature neuroscience. 2005; 8:752–758. [PubMed: 15895084]

Elder GA, Stone JR, Ahlers ST. Effects of low-level blast exposure on the nervous system: is there really a controversy? Frontiers in neurology. 2014; 5:269. [PubMed: 25566175]

Goldstein LE, Fisher AM, Tagge CA, Zhang XL, Velisek L, Sullivan JA, Upreti C, Kracht JM, Ericsson M, Wojnarowicz MW, Goletiani CJ, Maglakelidze GM, Casey N, Moncaster JA, Minaeva O, Moir RD, Nowinski CJ, Stern RA, Cantu RC, Geiling J, Blusztajn JK, Wolozin BL, Ikezu T, Stein TD, Budson AE, Kowall NW, Chargin D, Sharon A, Saman S, Hall GF, Moss WC, Cleveland RO, Tanzi RE, Stanton PK, McKee AC. Chronic traumatic encephalopathy in blast-exposed military veterans and a blast neurotrauma mouse model. Science translational medicine. 2012; 4:134ra160.

Hayes RL, Stalhammar D, Povlishock JT, Allen AM, Galinat BJ, Becker DP, Stonnington HH. A new model of concussive brain injury in the cat produced by extradural fluid volume loading: II. Physiological and neuropathological observations. Brain injury : [BI]. 1987; 1:93–112.

Hoffmann R, Lee VM, Leight S, Varga I, Otvos L Jr. Unique Alzheimer's disease paired helical filament specific epitopes involve double phosphorylation at specific sites. Biochemistry. 1997; 36:8114–8124. [PubMed: 9201960]

Huber BR, Meabon JS, Martin TJ, Mourad PD, Bennett R, Kraemer BC, Cernak I, Petrie EC, Emery MJ, Swenson ER, Mayer C, Mehic E, Peskind ER, Cook DG. Blast exposure causes early and persistent aberrant phospho- and cleaved-tau expression in a murine model of mild blast-induced traumatic brain injury. Journal of Alzheimer's disease : JAD. 2013; 37:309–323. [PubMed: 23948882]

Iliff JJ, Wang M, Liao Y, Plogg BA, Peng W, Gundersen GA, Benveniste H, Vates GE, Deane R, Goldman SA, Nagelhus EA, Nedergaard M. A paravascular pathway facilitates CSF flow through the brain parenchyma and the clearance of interstitial solutes, including amyloid beta. Science translational medicine. 2012; 4:147ra111.

Jiao Y, Sun Z, Lee T, Fusco FR, Kimble TD, Meade CA, Cuthbertson S, Reiner A. A simple and sensitive antigen retrieval method for free-floating and slide-mounted tissue sections. Journal of neuroscience methods. 1999; 93:149–162. [PubMed: 10634500]

Jorge RE, Acion L, White T, Tordesillas-Gutierrez D, Pierson R, Crespo-Facorro B, Magnotta VA. White matter abnormalities in veterans with mild traumatic brain injury. The American journal of psychiatry. 2012; 169:1284–1291. [PubMed: 23212059]

Jung S, Aliberti J, Graemmel P, Sunshine MJ, Kreutzberg GW, Sher A, Littman DR. Analysis of fractalkine receptor CX(3)CR1 function by targeted deletion and green fluorescent protein reporter gene insertion. Molecular and cellular biology. 2000; 20:4106–4114. [PubMed: 10805752]

Kim HJ, Chang KA, Ha TY, Kim J, Ha S, Shin KY, Moon C, Nacken W, Kim HS, Suh YH. S100A9 knockout decreases the memory impairment and neuropathology in crossbreed mice of Tg2576 and S100A9 knockout mice model. PloS one. 2014; 9:e88924. [PubMed: 24586443]

Koliatsos VE, Cernak I, Xu L, Song Y, Savonenko A, Crain BJ, Eberhart CG, Frangakis CE, Melnikova T, Kim H, Lee D. A Mouse Model of Blast Injury to Brain: Initial Pathological, Neuropathological, and Behavioral Characterization. Journal of neuropathology and experimental neurology. 2011; 70:399–416. [PubMed: 21487304]

Lighthall JW. Controlled Cortical Impact: A New Experimental Brain Injury Model. Journal of neurotrauma. 1988; 5:1–15. [PubMed: 3193461]

London A, Itskovich E, Benhar I, Kalchenko V, Mack M, Jung S, Schwartz M. Neuroprotection and progenitor cell renewal in the injured adult murine retina requires healing monocyte-derived macrophages. The Journal of experimental medicine. 2011; 208:23–39. [PubMed: 21220455]

Mac Donald CL, Johnson AM, Cooper D, Nelson EC, Werner NJ, Shimony JS, Snyder AZ, Raichle ME, Witherow JR, Fang R, Flaherty SF, Brody DL. Detection of blast-related traumatic brain injury in U.S. military personnel. The New England journal of medicine. 2011; 364:2091–2100. [PubMed: 21631321]

Magnoni S, Esparza TJ, Conte V, Carbonara M, Carrabba G, Holtzman DM, Zipfel GJ, Stocchetti N, Brody DL. Tau elevations in the brain extracellular space correlate with reduced amyloid-beta levels and predict adverse clinical outcomes after severe traumatic brain injury. Brain : a journal of neurology. 2012; 135:1268–1280. [PubMed: 22116192]

McKee AC, Stein TD, Nowinski CJ, Stern RA, Daneshvar DH, Alvarez VE, Lee HS, Hall G, Wojtowicz SM, Baugh CM, Riley DO, Kubilus CA, Cormier KA, Jacobs MA, Martin BR, Abraham CR, Ikezu T, Reichard RR, Wolozin BL, Budson AE, Goldstein LE, Kowall NW, Cantu RC. The spectrum of disease in chronic traumatic encephalopathy. Brain : a journal of neurology. 2013; 136:43–64. [PubMed: 23208308]

McPherson CA, Merrick BA, Harry GJ. In vivo molecular markers for pro-inflammatory cytokine M1 stage and resident microglia in trimethyltin-induced hippocampal injury. Neurotox Res. 2014; 25:45–56. [PubMed: 24002884]

Morrison HW, Filosa JA. A quantitative spatiotemporal analysis of microglia morphology during ischemic stroke and reperfusion. Journal of neuroinflammation. 2013; 10:4. [PubMed: 23311642]

Nimmerjahn A, Kirchhoff F, Helmchen F. Resting microglial cells are highly dynamic surveillants of brain parenchyma in vivo. Science. 2005; 308:1314–1318. [PubMed: 15831717]

Nimmerjahn A, Kirchhoff F, Kerr JN, Helmchen F. Sulforhodamine 101 as a specific marker of astroglia in the neocortex in vivo. Nature methods. 2004; 1:31–37. [PubMed: 15782150]

Nitta T, Hata M, Gotoh S, Seo Y, Sasaki H, Hashimoto N, Furuse M, Tsukita S. Size-selective loosening of the blood-brain barrier in claudin-5-deficient mice. The Journal of cell biology. 2003; 161:653–660. [PubMed: 12743111]

Omalu B, Hammers JL, Bailes J, Hamilton RL, Kamboh MI, Webster G, Fitzsimmons RP. Chronic traumatic encephalopathy in an Iraqi war veteran with posttraumatic stress disorder who committed suicide. Neurosurgical focus. 2011; 31:E3.

Owens BD, Kragh JF Jr, Wenke JC, Macaitis J, Wade CE, Holcomb JB. Combat wounds in operation Iraqi Freedom and operation Enduring Freedom. The Journal of trauma. 2008; 64:295–299. [PubMed: 18301189]

Perez-Polo JR, Rea HC, Johnson KM, Parsley MA, Unabia GC, Xu G, Infante SK, Dewitt DS, Hulsebosch CE. Inflammatory consequences in a rodent model of mild traumatic brain injury. Journal of neurotrauma. 2013; 30:727–740. [PubMed: 23360201]

Petrie EC, Cross DJ, Yarnykh VL, Richards T, Martin NM, Pagulayan K, Hoff D, Hart K, Mayer C, Tarabochia M, Raskind MA, Minoshima S, Peskind ER. Neuroimaging, behavioral, and psychological sequelae of repetitive combined blast/impact mild traumatic brain injury in Iraq and Afghanistan war veterans. Journal of neurotrauma. 2014; 31:425–436. [PubMed: 24102309]

Plog BA, Dashnaw ML, Hitomi E, Peng W, Liao Y, Lou N, Deane R, Nedergaard M. Biomarkers of traumatic injury are transported from brain to blood via the glymphatic system. The Journal of neuroscience : the official journal of the Society for Neuroscience. 2015; 35:518–526. [PubMed: 25589747]

Readnower RD, Chavko M, Adeeb S, Conroy MD, Pauly JR, McCarron RM, Sullivan PG. Increase in blood-brain barrier permeability, oxidative stress, and activated microglia in a rat model of blast-induced traumatic brain injury. Journal of neuroscience research. 2010; 88:3530–3539. [PubMed: 20882564]

Roth TL, Nayak D, Atanasijevic T, Koretsky AP, Latour LL, McGavern DB. Transcranial amelioration of inflammation and cell death after brain injury. Nature. 2014; 505:223–228. [PubMed: 24317693]

Seiffert E, Dreier JP, Ivens S, Bechmann I, Tomkins O, Heinemann U, Friedman A. Lasting blood-brain barrier disruption induces epileptic focus in the rat somatosensory cortex. The Journal of neuroscience : the official journal of the Society for Neuroscience. 2004; 24:7829–7836. [PubMed: 15356194]

Shechter R, London A, Varol C, Raposo C, Cusimano M, Yovel G, Rolls A, Mack M, Pluchino S, Martino G, Jung S, Schwartz M. Infiltrating Blood-Derived Macrophages Are Vital Cells Playing an Anti-inflammatory Role in Recovery from Spinal Cord Injury in Mice. PLoS Med. 2009; 6:e1000113. [PubMed: 19636355]

Wang G, Zhang J, Hu X, Zhang L, Mao L, Jiang X, Liou AK, Leak RK, Gao Y, Chen J. Microglia/macrophage polarization dynamics in white matter after traumatic brain injury. Journal of cerebral blood flow and metabolism : official journal of the International Society of Cerebral Blood Flow and Metabolism. 2013; 33:1864–1874.

Xie L, Kang H, Xu Q, Chen MJ, Liao Y, Thiyagarajan M, O'Donnell J, Christensen DJ, Nicholson C, Iliff JJ, Takano T, Deane R, Nedergaard M. Sleep drives metabolite clearance from the adult brain. Science. 2013; 342:373–377. [PubMed: 24136970]

Xu H-T, Pan F, Yang G, Gan W-B. Choice of cranial window type for in vivo imaging affects dendritic spine turnover in the cortex. Nature neuroscience. 2007; 10:549–551. [PubMed: 17417634]

Yang G, Pan F, Parkhurst CN, Grutzendler J, Gan W-B. Thinned-skull cranial window technique for long-term imaging of the cortex in live mice. Nat Protocols. 2010; 5:201–208. [PubMed: 20134419]

Yoshiyama Y, Higuchi M, Zhang B, Huang SM, Iwata N, Saido TC, Maeda J, Suhara T, Trojanowski JQ, Lee VM. Synapse loss and microglial activation precede tangles in a P301S tauopathy mouse model. Neuron. 2007; 53:337–351. [PubMed: 17270732]

Zujovic V, Benavides J, Vigé X, Carter C, Taupin V. Fractalkine modulates TNF-α secretion and neurotoxicity induced by microglial activation. Glia. 2000; 29:305–315. [PubMed: 10652441]

Highlights

- Mild blast exposure elicits focal microdomains of brain microvessel dysfunction.
- Blast-induced microvessel dysfunction can start to develop hours after the initial blast exposure.
- Microglia/macrophage activation is closely associated with microvessel dysfunction microdomains and aberrant tight junction morphology.
- A single mild blast exposure is sufficient to induce transient perivascular phospho-tau accumulation.

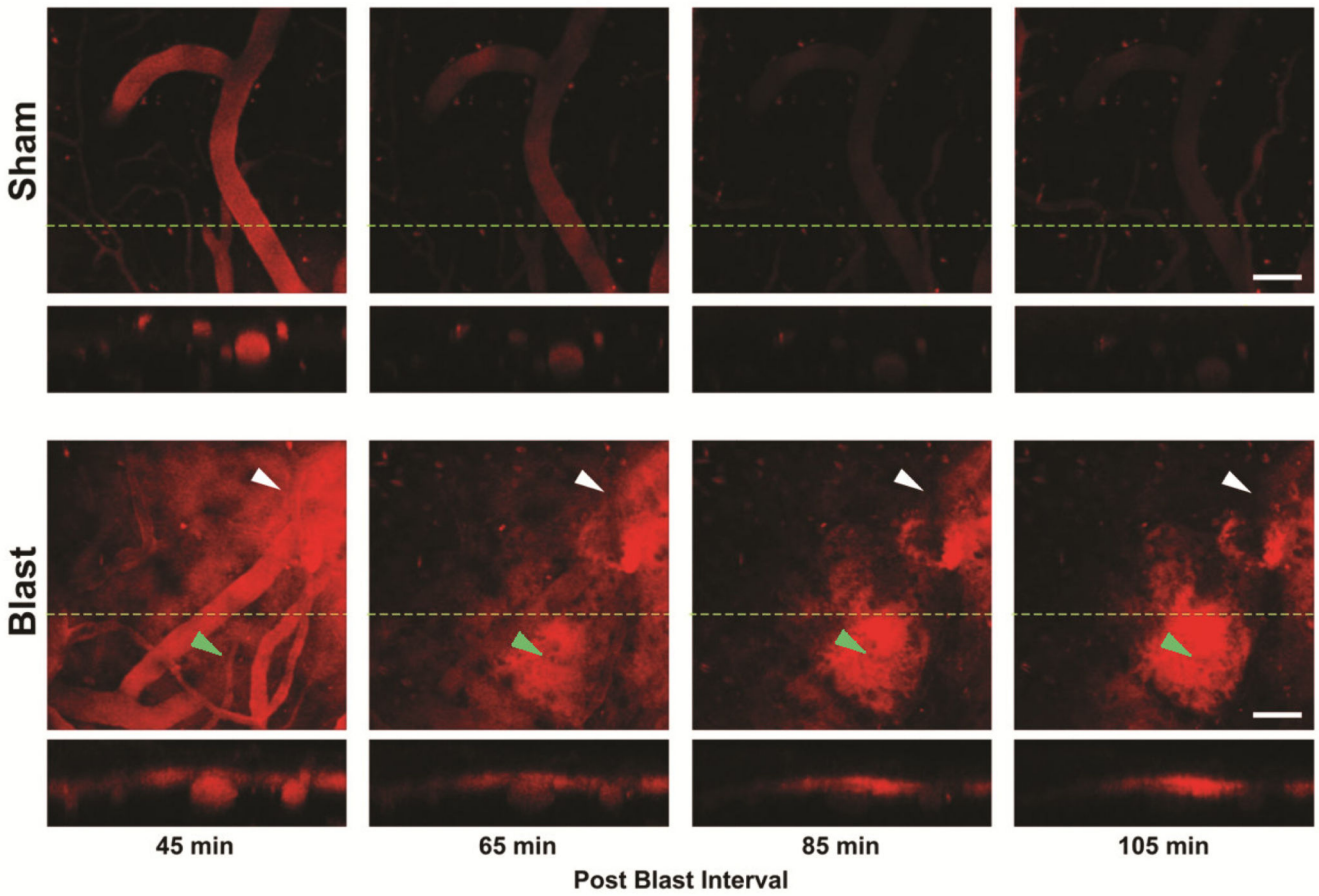

Figure 1. Mild blast exposure causes dynamic microdomains of blood-brain barrier disruption

Real-time two-photon intravital imaging revealed that peripherally injected intravascular Quantum dots$_{655}$ were restricted to the microvessels of sham-treated control mice. The perpendicular slice (indicated by a dashed green line) through the cortex is shown in the lower panels to further confirm that the QDots$_{655}$ remained inside both pial vessels and microvessels deeper in the cortical parenchyma. Imaging was begun 45 minutes after a single mild BOP, a microdomain of vascular disruption can be seen where QDots$_{655}$ escaped the endothelium into the surrounding parenchyma and accumulated in the subpial Virchow-Robin space (white arrowhead). A second microdomain developed 105 minutes after blast exposure (green arrowhead). The image represents the largest field of view common to all frames with slight formatting adjustments. Scale bars: 50 μm.

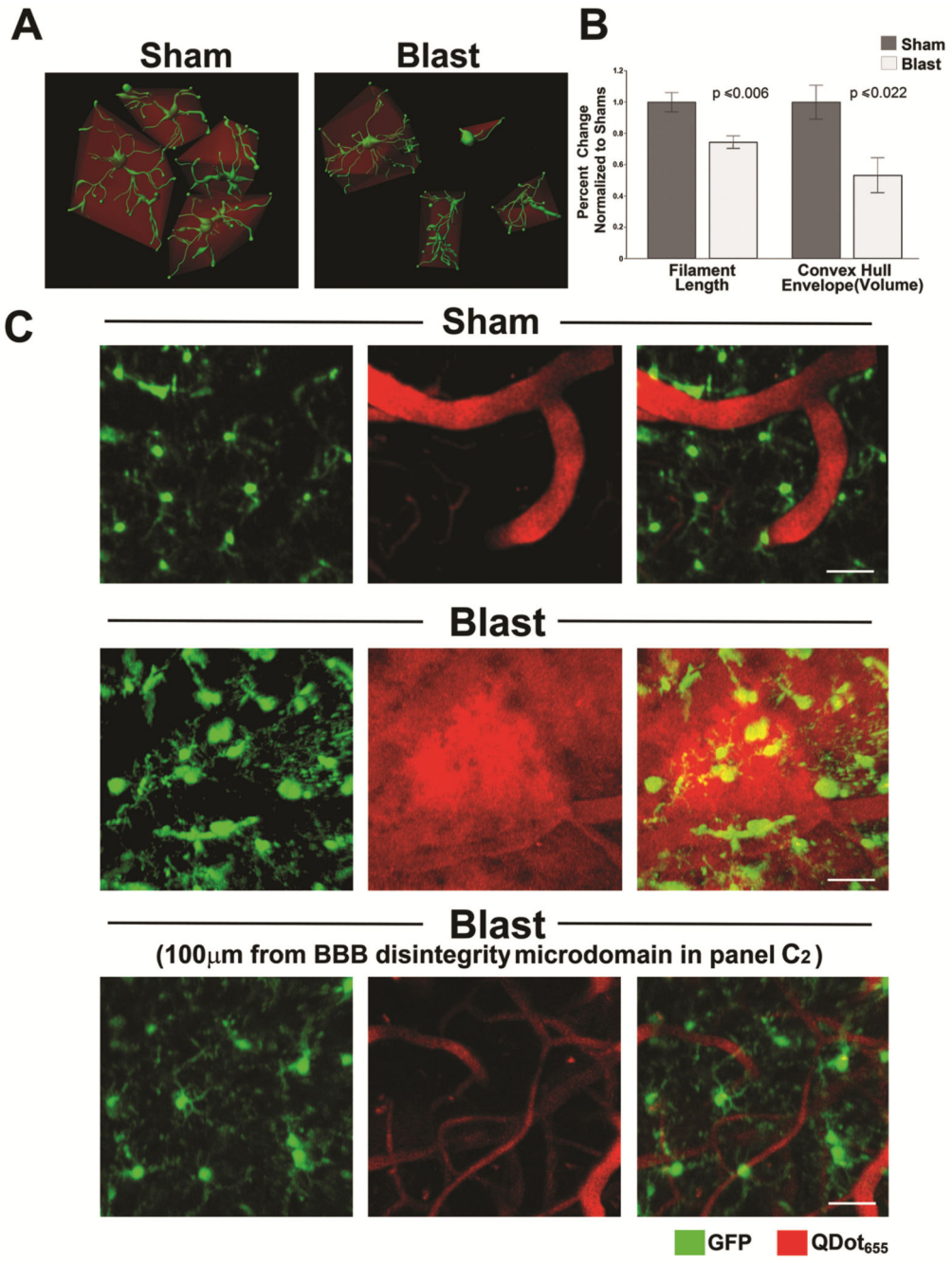

Figure 2. Mild blast-induced cortical vascular disruption microdomains cause region specific microglia/macrophage activation in CX3CR1-GFP$^{+/-}$ mice

(A) A single mild blast exposure caused microglia/macrophages to rapidly adopt morphology consistent with a state of activation. *In vivo* two-photon microscopy was performed on sham and blast-exposed CX3CR1-GFP$^{+/-}$ mice expressing GFP in microglia/macrophages (green). Microglia/macrophages were imaged within the cortical CNS parenchyma 45 minutes post-treatment. Figure depicts reconstructed 3-D microglial/macrophage morphology derived from *in vivo* two-photon image stacks analyzed by Imaris

software (see Methods) to identify individual cells, then determine cellular, morphology, process length, and calculate an encapsulating convex hull volume (red). **(B)** Results of this analysis revealed that blast significantly decreased filament length ($p<0.006$, N=6 and 4, BOP and sham, respectively) and convex hull volume in blast-exposed mice compared to shams ($p<0.022$, N=6 and 4, BOP and sham, respectively). **(C)** Microglia in sham-treated CX3CR1-GFP$^{+/-}$ animal (upper panel) demonstrated mostly thin, ramified processes with no evidence of aberrant peripherally injected QDots$_{655}$ escaping microvessels. Middle panel shows that mild blast caused vascular disruption with QDots$_{655}$ escaping into surrounding parenchyma and accompanied by microglia process retraction and microglia/macrophages adopting rounded amoeboid morphology consistent with an activated state. Lower panel shows images from the same blast-exposed animal approximately 100μm from the microdomain of vascular disruption shown above with less activated-appearing microglia/macrophages compared to middle panel. Scale bars: 40 μm.

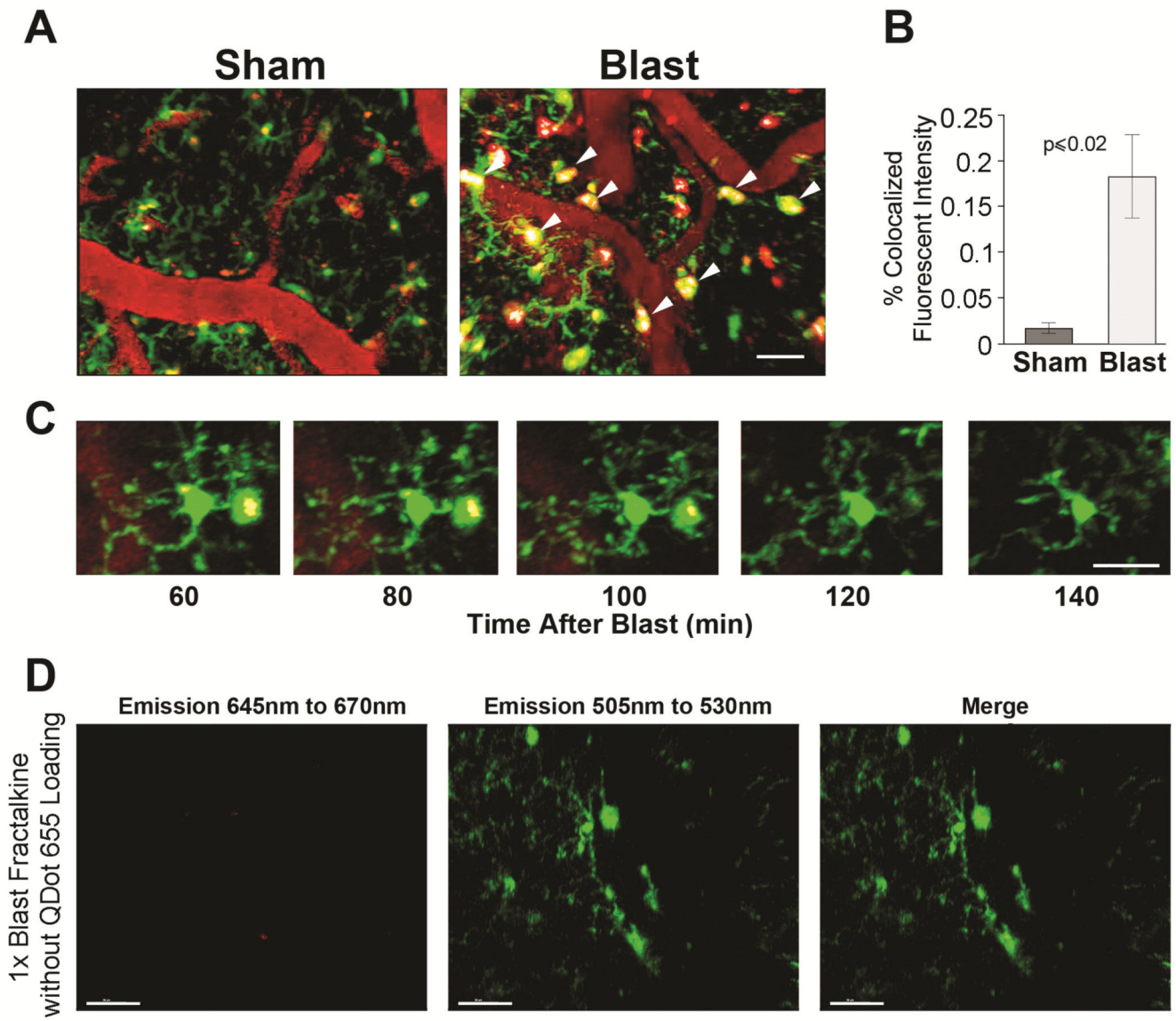

Figure 3. Blast-exposed microglia accumulate Qdots in cell bodies and phagosome-like juxtavascular processes

(**A**) In CX3CR1-GFP$^{+/-}$ mice, QDots$_{655}$ (red) remained predominantly in microvessels in sham-treated mice. In 1X blast-exposured animals, QDots$_{655}$ crossing the endothelium accumulated in juxtavascular processes and somas of microglia/macrophages (green). QDots$_{655}$ colocalized with microglia/macrophages denoted by arrowheads. Other red puncta not colocalizing with GFP-positive cells is likely indicative of damaged/fragmented cells. (**B**) Mild blast caused a significant increase in Qdots$_{655}$ internalized in microglia/macrophages compared to sham treated animals ($p< 0.02$). (**C**) Time lapse image series (60–140 min post-blast) show phagocytosed QDots$_{655}$ accumulating in enlarged perivascular processes extending from a microglial cell body. (**D**) Lack of QDots$_{655}$ emissions (645 nm to 670 nm) in CX3CR1-GFP$^{+/-}$ mice (emissions at 505nm to 530nm) without QDots$_{655}$

confirms that QDot colocalization in GFP-expressing cells is specific and not due to non-specific auto-flourescence. Scale bars: (A, C) 20 μm, (D) 30 μm.

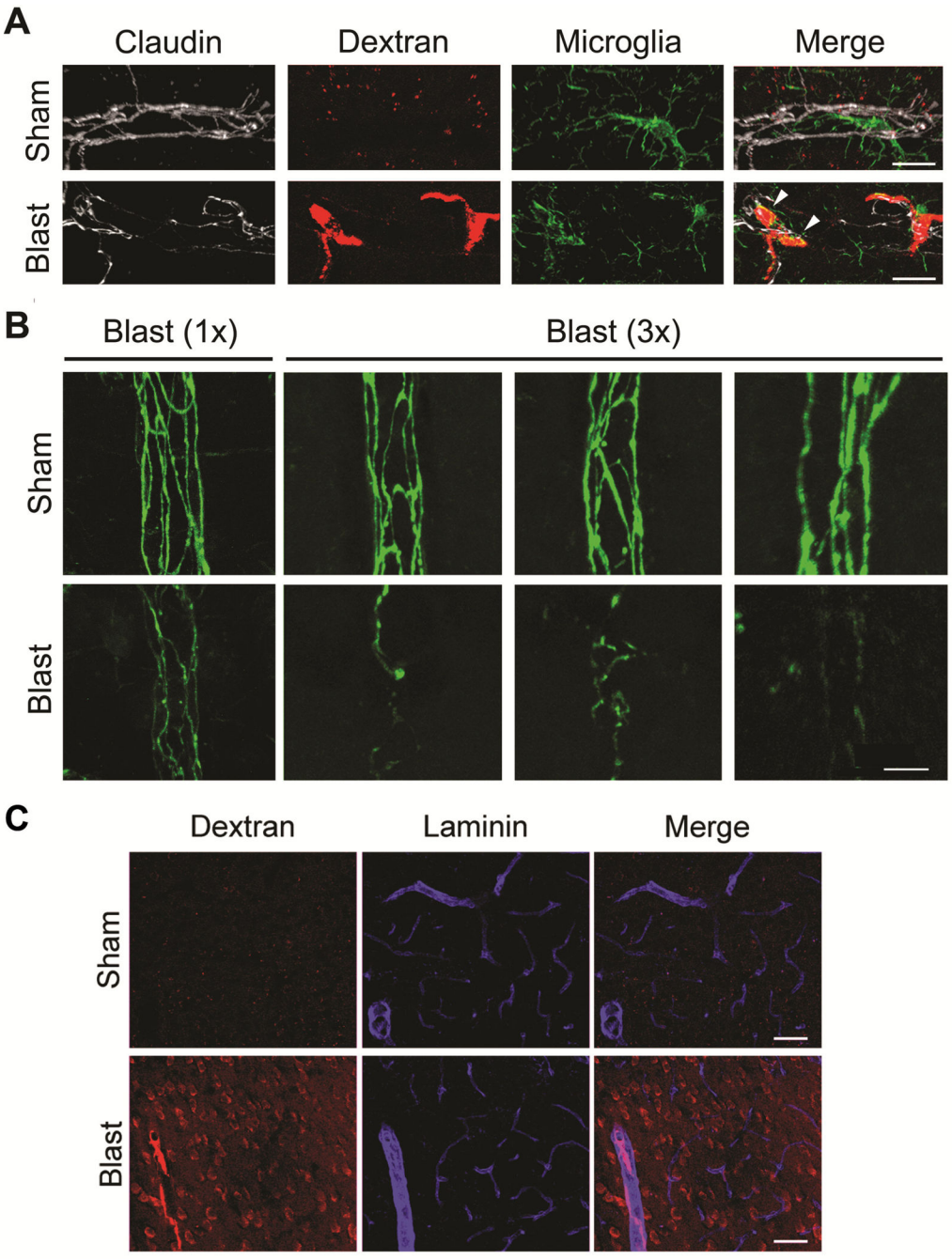

Figure 4. Discontinuous tight junction morphology and endothelial disruption induced by mild blast

All images show maximum-field projections of 40 serially acquired images scanned at 1 μm intervals in the Z-plane (40 μm total tissue thickness) in cortex of fixed, immunostained sections from wild-type C57BL6 mice. (**A**) Triple-label confocal microscopy shows tight junctional claudin-5 (white pseudo color) and microglial/macrophage Iba-1 (green) immunoreactivity, as well as 10 kDa dextran (red) that had crossed the BBB one hour post blast. In contrast to sham (upper panel), 1X blast exposure caused focal vascular disruption evidenced by escape of 10 kDa dextran into the surrounding paranchyma (arrowheads)

associated with aberrant tight junction claudin-5 morphology and activated-appearing microglia/macrophages. (**B**) Claudin-5 immunostaining in sham-treated animals (24 hours post-treatment) revealed normal appearing tight junction morphology in cortical penetrating vessels. At 24 hours after a single (1X) blast exposure, disturbed tight junction morphology was markedly less pronouced than at 4 hours after 1X blast-exposure as in Panel A. However, following repetitive 3X blast exposure claudin-5 immunostained tight junctions appear discontinuous and irregular compared to shams. (**C**) Even though 1X blast induced transiently disturbed tight junction morphology, within 1 hour peripherally-injected 10kDa dextran escapes into the cortical parenchyma (images representative of 3/4 blast-exposed animals and 4/4 shams). Scale bars: (A) 20 μm, (B) 10 μm. (C) 40 μm.

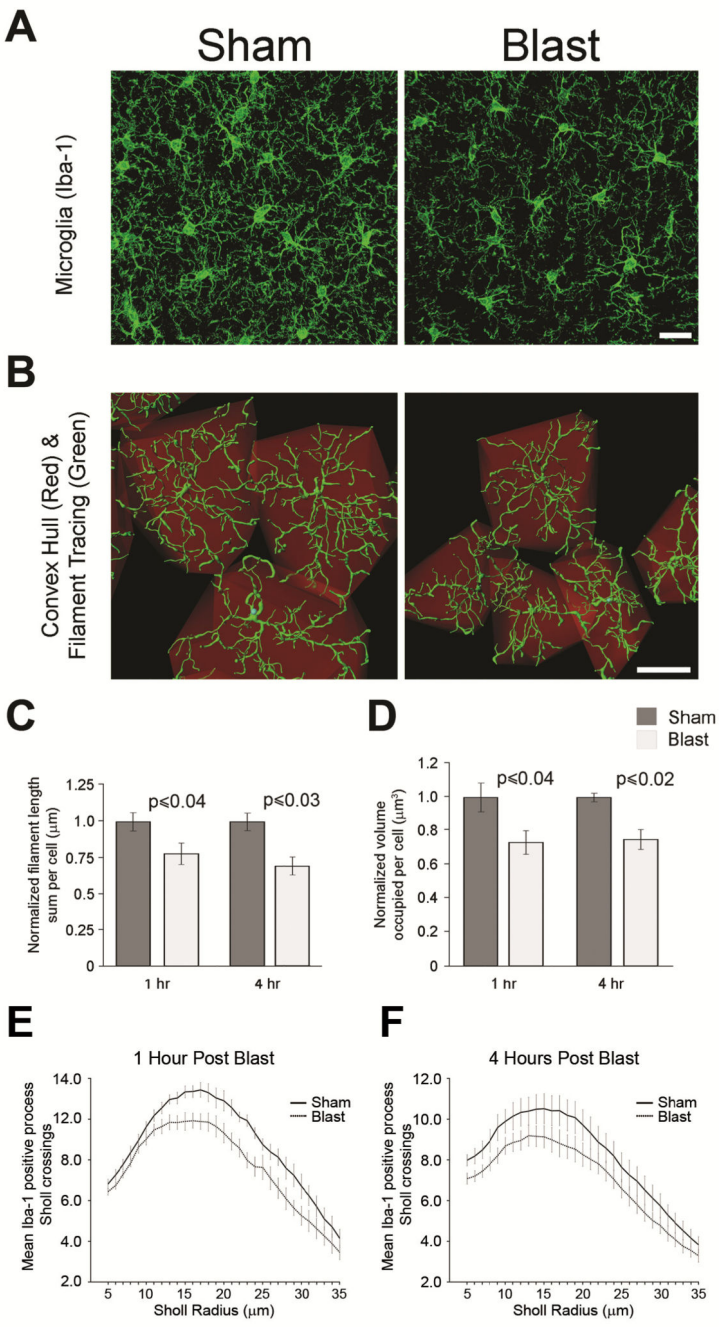

Figure 5. Blast exposure causes microglial morphological alterations

(**A**) Confocal microscopy of fixed cortical tissue shows that Iba-1 immunostained microglia (green) in wild-type C57BL6 1X blast-exposed cortex have fewer processes compared to sham controls. (**B**) In cortex (150–500 μm below cortical surface) of wild-type C57BL6 mice, reconstructed 3-D microglial/macrophage morphology derived from confocal image stacks of fixed tissue shows Iba-1 immuno-positive (green) cellular morphology, process length, and convex hull volume (red). Microglia-encapsulating complex hull volume was reduced in blast exposed C57BL6 mice compared to shams. (**C**) Histogram shows microglia

filament length was significantly reduced at 1 hour ($p \leq 0.04$, N= 5 and 5, BOP and sham respectively) and 4 hours ($p \leq 0.03$, N= 4 and 4, BOP and sham, respectively) after 1X blast exposure compare to shams. (**D**) Convex hull volume was significantly reduced at 1 hour ($p \leq 0.04$, N=5 and 5, BOP and sham, respectively) and 4 hours ($p \leq 0.02$, N=4 and 4, BOP and sham, respectively) after 1X blast compare to controls. Sholl analysis of Iba-1 immunostained cortical microglia evaluated at 1 (**E**) and 4 (**F**) hours post-treatment revealed a significant decrease in the mean number of Sholl crossings in 1X blast-exposed mice compared to shams ($p \leq 0.022$, N=5 animals per group). Error bars denote ±s.e.m. Scale bars: 20 μm.

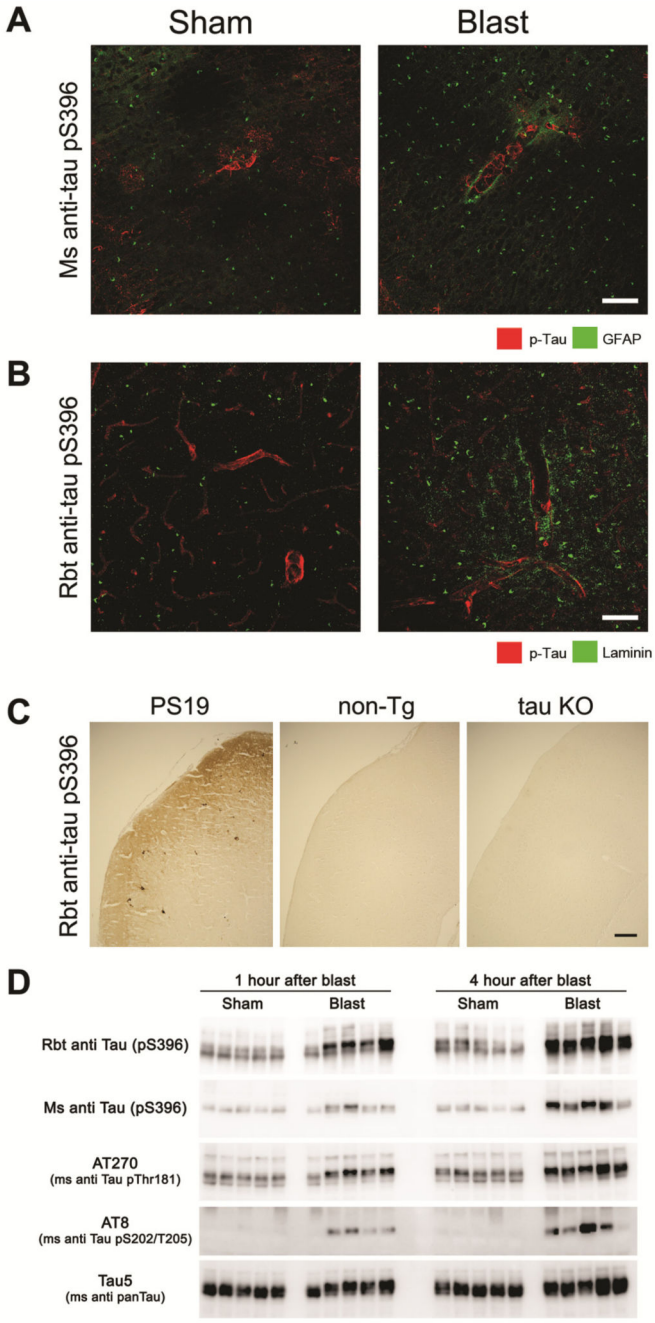

Figure 6. Mild blast exposure causes transient perivascular phospho-tau accumulation

(**A**) One hour following a single BOP, phospho-tau (detected by a well-characterized mouse monoclonal anti-phospho-tau S396 antibody, green) aberrantly accumulated around cortical microvessels highlighted by a sheath of endfoot GFAP immunoreactivity (red). (**B**) Confirmatory immunostaining with a rabbit anti-tau pS396 antibody also revealed altered perivascular phospho-tau expression (green) following blast, with the microvascular space delineated by laminin immunoreactivity (red). (**C**) Validating the specificity of the less-well characterized rabbit tau-pS396 antibody, phospho-tau deposits in transgenic PS19 mice

expressing mutant (P301S) tau were immunopositive, whereas cortical tissue from non-transgenic (non-Tg) mice and tau-deficient (tau KO) mice were immunonegative. (**D**). Western blots show that in cortex, a single mild blast exposure caused markedly increased expression of multiple indicated phospho-tau species at both 1 and 4 hours, while total tau levels (Tau5 in lower panel) were comparable among shams and BOP-exposed animals (each lane indicates results from one mouse, N=5 and 5, sham and blast-exposed, respectively). Scale bars: (A, B) 20 μm, (C) 100 μm.

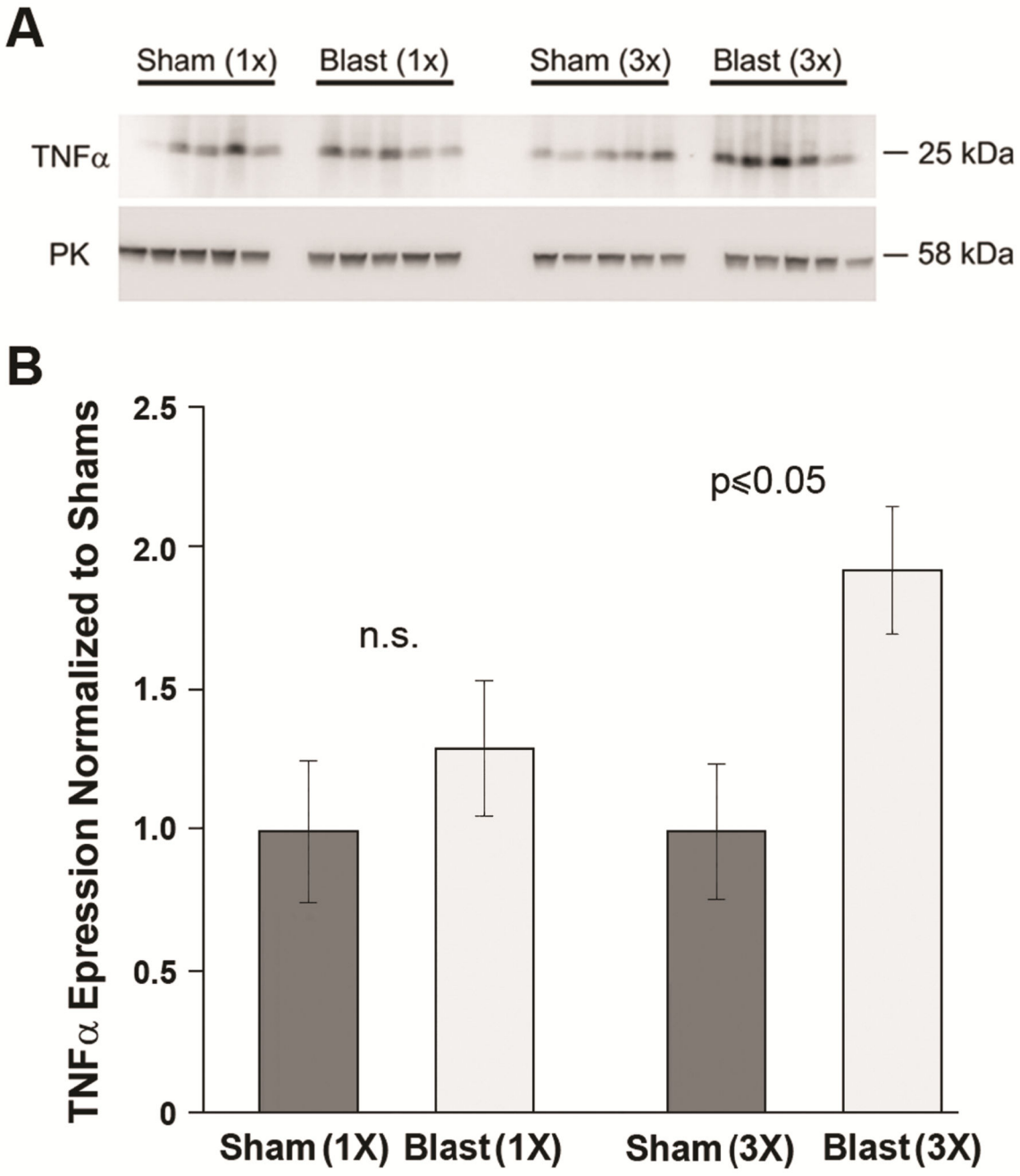

Figure 7. Repetitive blast exposure causes persistant increases in TNFα

(**A**) Western blots indicate TNFα protein expression was elevated 14 days following repetitive (3X), but not after single (1X) blast exposure (N=5 for each group). Lower panel shows pyruvate kinase (PK) levels that served as protein load control. (**B**) Histogram shows normalized TNFα protein expression levels were significantly elevated in 3X ($p \leq 0.05$), but not 1X blast exposure (non-significant, n.s.) compared to shams.